Michigan Technological University

Michigan Technological University
Digital Commons @ Michigan Tech

Department of Physics Publications | Department of Physics

3-30-2015

On the variability of drop size distributions over areas

A. R. Jameson
RJH Scientific, Inc., El Cajon, California

M. L. Larsen
College of Charleston

A. B. Kostinski
Michigan Technological University

Follow this and additional works at: https://digitalcommons.mtu.edu/physics-fp

 Part of the Physics Commons

Recommended Citation

Jameson, A. R., Larsen, M. L., & Kostinski, A. B. (2015). On the variability of drop size distributions over areas. *Journal of the Atmospheric Sciences, 76*(3), 1387-1397. http://dx.doi.org/10.1175/JAS-D-14-0258.1

Retrieved from: https://digitalcommons.mtu.edu/physics-fp/175

Follow this and additional works at: https://digitalcommons.mtu.edu/physics-fp

 Part of the Physics Commons

On the Variability of Drop Size Distributions over Areas

A. R. JAMESON

RJH Scientific, Inc., El Cajon, California

M. L. LARSEN

College of Charleston, Charleston, South Carolina

A. B. KOSTINSKI

Michigan Technological University, Houghton, Michigan

(Manuscript received 6 September 2014, in final form 25 December 2014)

ABSTRACT

Past studies of the variability of drop size distributions (DSDs) have used moments of the distribution such as the mass-weighted mean drop size as proxies for the entire size distribution. In this study, however, the authors separate the total number of drops N_t from the DSD leaving the probability size distributions (PSDs); that is, DSD = $N_t \times$ PSD. The variability of the PSDs are then considered using the frequencies of size [$P(D)$] values at each different drop diameter $P(P_D \mid D)$ over an ensemble of observations collected using a network of 21 optical disdrometers. The relative dispersions R_D of $P(P_D \mid D)$ over all the drop diameters are used as a measure of PSD variability. An intrinsic PSD is defined as an average over one or more instruments excluding zero drop counts. It is found that variability associated with an intrinsic PSD fails to characterize its true variability over an area. It is also shown that this variability is not due to sampling limitations but rather originates for physical reasons. Furthermore, this variability increases with the expansion of the network size and with increasing drop diameter.

A physical explanation is that the network acts to integrate the Fourier transform of the spatial correlation function from smaller toward larger wavelengths as the network size increases so that the contributions to the variance by all spatial wavelengths being sampled also increases. Consequently, R_D and, hence, PSD variability will increase as the size of the area increases.

1. Introduction

Ever since the first reports of the frequency distribution of drops of various sizes [i.e., drop size distributions (DSDs)] (Laws and Parsons 1943; Marshall and Palmer 1948; Best 1950), there has been a growing appreciation of their variability particularly with regard to different meteorological conditions. For decades, a great deal of effort has been spent characterizing DSDs of all kinds, so much so that there are now hundreds and possibly thousands of expressions. Moreover, to a large extent, the appearance of the field of radar meteorology arose in response to DSDs because the integral properties of the radar reflectivity factor Z and the rainfall rate R could be directly connected, thus making radar a potentially practical instrument for rapidly measuring rain over large areas. While this potential is still being explored today, the variability of the DSDs not only has led to a vast family of Z–R relations, but the DSDs have also produced families of parameterizations that relate the variables of the DSDs to their integral properties. Unfortunately, such parameterizations, by their very nature, tend to minimize a full appreciation of the true variability of the underlying DSDs.

This is not to say that such variability is not appreciated particularly as it impacts radar reflectivity factor, beginning with Wexler (1948) and Jones (1956) up to the present (e.g., Islam et al. 2012a,c), and rainfall spatial distributions (e.g., Lee and Zawadzki 2005; Lee et al.2009; Tokay and Bashor 2010; Jaffrain and Berne 2012a). These

Corresponding author address: A. R. Jameson, 5625 N. 32nd St., Arlington, VA 22207-1560.
E-mail: arjatrjhsci@verizon.net

DOI: 10.1175/JAS-D-14-0258.1

© 2015 American Meteorological Society

past studies, however, only use variability of the moments of a size distribution as a proxy for the variability of the entirety of the DSDs themselves.

Furthermore, more recently Jaffrain and Berne (2012b) have proposed a decreasing stretched exponential function to describe the spatial correlation for DSD integrated parameters for detector separations greater than 100 m. What this means with regard to the high temporal and spatial resolution of the DSDs themselves is not clear, however. As important as such studies are for many practical purposes, so far no one has considered looking directly at the variability of the DSDs at each drop size on scales less than 100 m as we do in this study.

As just mentioned, DSD variability has often been evaluated using integrated quantities such as the mean diameter. This is inadequate, however. Integrated variables depend not only on the form of the DSD but also on the limits of the integration. Thus, the same value of the integrated variable can be produced by a wide variety of different DSDs. Consequently, the variability of integrated quantities fails to capture the total variability of the DSDs. So what do we mean here by DSD variability? Normally, one has access to time series measurements using a single instrument, and normally elements of the time series are averaged to reduce fluctuations arising as a result of a variable number of drops at all different sizes. Hence, there is variability due to sampling and that due to real physics. We will show below that it is the latter that dominates over a network.

Specifically, a drop size distribution can be described as the product of the total number of drops N_t times the frequency distribution of drops with size $P(D)$ as argued in Kostinski and Jameson (1999); that is, $N(D)dD = N_t P(D)dD$, where $P(D)dD$ is the probability of finding a drop size between D and $D + dD$. That is, DSD = $N_t \times$ PSD, where PSD = $P(D)$. While N_t plays a critical role in the variability of the rainfall rate and other quantities (e.g., Jameson and Kostinski 2001; Jameson 2015; Jameson et al. 2015), the focus here is on the variability in the frequencies of different sizes of drops—that is, on the variability of $P(D)$. Specifically, one takes the observed drop counts at the different size bins using a disdrometer, whether impact or optical, and normalizes the count at each drop size by N_t to yield the estimate of $P(D)$, the frequency or probability distribution of drop sizes. From observation to observation, $P(D) = P_D$ varies at each D. We then have a probability distribution of the different values of PSD at each D denoted by $P(P_D \mid D)$. Thus, the variability of the PSD is equivalent to the variability of $P(D)$ at each size over all sizes over an ensemble of measurements. Hence, in this work, when we speak of the variability of the drop size distribution, we mean the spread or relative dispersion in the values of $P(P_D \mid D)$ at all the different drop sizes relative to their mean $P(D)$. Later, we also provide a measure over an entire network of instruments.

Below we describe a network of 21 optical disdrometers used to explore the variability of PSD. There are two ways of looking at these data. The first is to combine all the observations so that each instrument contributes to a distribution of $P(D)$ at each size. What, then, is the average PSD regardless of the location of the instrument? In effect, this excludes all $P(D) = 0$ that contribute no information. [For example, in the extreme case when all $P(D) = 0$, there is nothing to talk about.] Then at each drop size, there will be an ''intrinsic'' relative dispersion of $P(P_D \mid D)$ reflecting the variability of $P(D)$ at each D excluding all zeros.

The second way of considering the data is to ask, ''What is the average drop size distribution over the area of the network each minute?'' That is, what happens when one takes an intrinsic PSD and distributes it spatially over an area? Now, the occurrences of $P(D) = 0$ are meaningful since voids can occur within the area encompassed by a network. Such variability impacts the answer to that question. This distinction, while seemingly academic, can strongly influence the network-relative dispersions of $P(P_D \mid D)$ at each size and, consequently, the potential variability of the network-average PSD. This will be discussed further below.

While seemingly pedantic, this distinction is important when one wants to consider rainfall over an area because the intrinsic $P(D)$ alone does not fully account for the effects of spatial variability particularly the spatial voids, which may appear at different sizes at different locations and times. Obviously, integration time will influence but not eliminate the occurrences and locations of these voids since they are not all due to sampling fluctuations. To provide an illustration of such spatial variability, Fig. 1 shows the PSDs [$P(D)$] observed every minute by two detectors over a 440-min rain event consisting of both intense rain from thunderstorms and light rain from subsequent anvil containing a few weak, transient intense elements discussed further below. Even though the two identical instruments are separated by only 1.93 m, the profiles of $P(D)$ can still be significantly different (aside from instrument differences) as indicated in Fig. 1c and as discussed further later. These differences (Fig. 1a) between the two PSDs were not influenced by any statistically significant bias in N_t between these two detectors for these data (Fig. 1d).

In the next section, we describe the network in greater detail, provide a few definitions, and establish the connection between the relative dispersions of $P(P_D \mid D)$ at each D and the variability in both the intrinsic and the

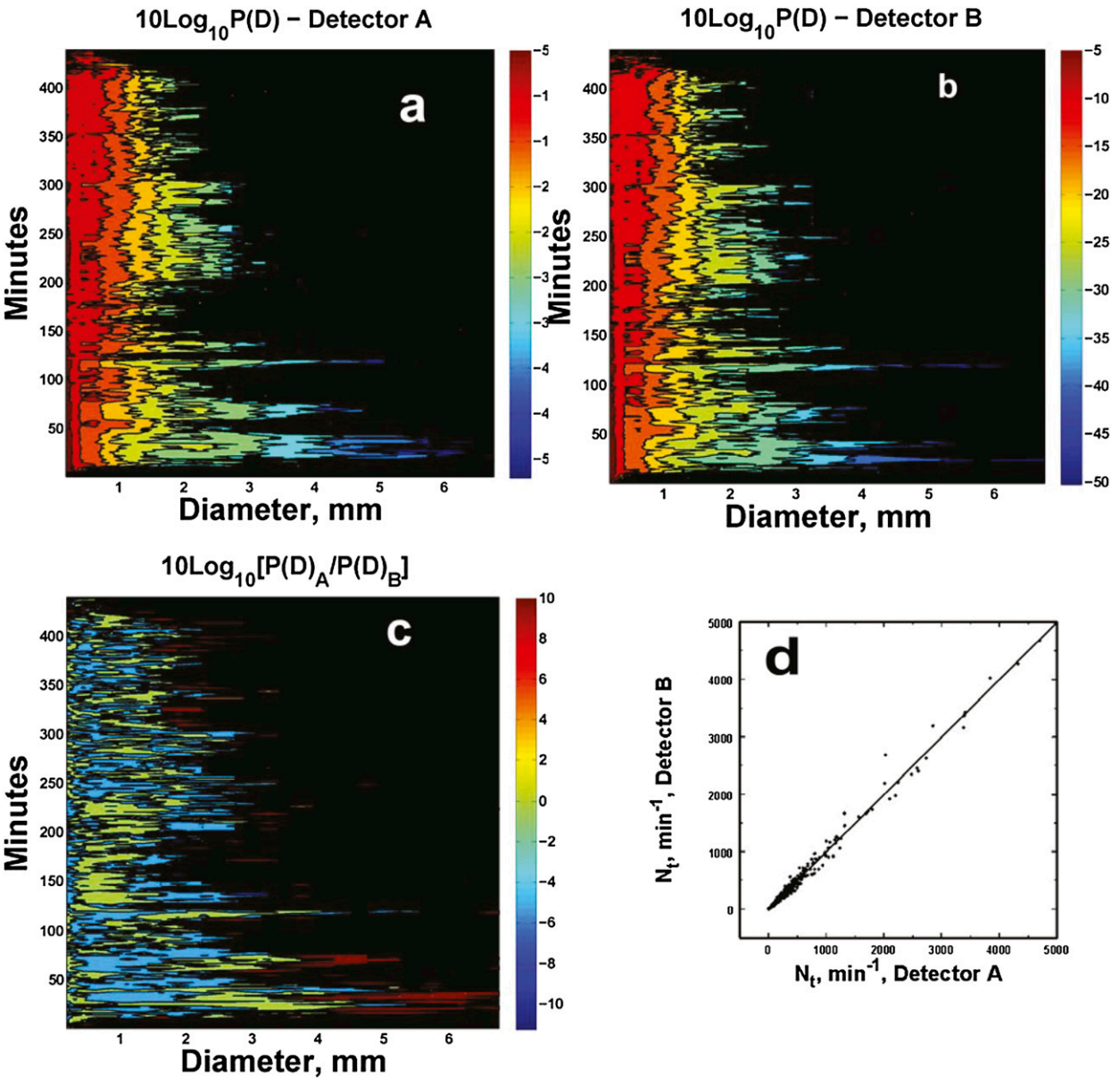

FIG. 1. A contour plot of $\log_{10}[P(D)]$ over the entire 440-min rain event for two optical disdrometers in the network (see Fig. 2): (a) optical disdrometer A and (b) optical disdrometer B, only 1.93 m away from A. (c) A plot of the ratio of the two $P(D)$ highlighting differences between the two detectors. (d) The scatterplot between N_t for detectors A and B showing no bias.

network-average PSDs. Data analyses and results will then follow.

2. Preliminary considerations

a. The network of detectors

The network consists of 21 Thies Laser Precipitation Monitors (LPMs), in conjunction with a Joanneum compact two-dimensional video disdrometer (2DVD). The array is located at historic Dixie Plantation near Hollywood, South Carolina; this property (owned by the College of Charleston Foundation) is used for a variety of ecological, educational, and research purposes. The site is located at 32°44′26″N, 80°10′36″W.

The instrument layout is shown in Fig. 2 and was designed to develop a dense network with distinct spatial separations. This layout contrasts with the usual grid setup that collects a lot of information at only one a particular separation distance but then abandons

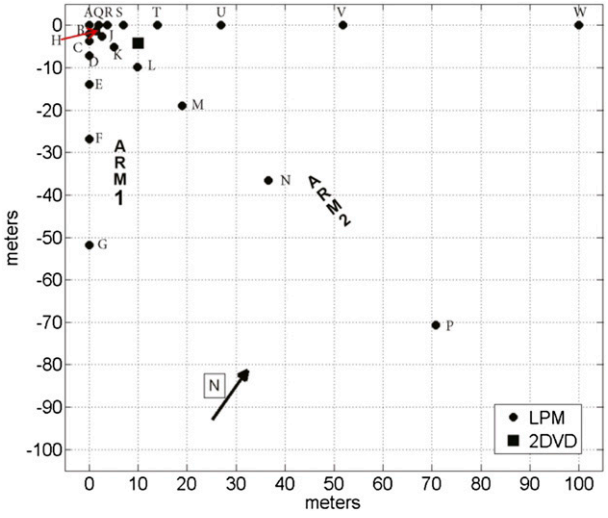

FIG. 2. A schematic of the layout of the LPM (optical disdrometers) network, with the letters referencing specific instruments as further discussed in the text. The 2DVD is indicated by the square. The origin of the network is taken to be at detector A in the upper-left corner. The arms refer to specific linear arrays of instruments.

information on many other scales. By using logarithmic spacing, however, spatial scales from approximately 1 to 100 m can be explored simultaneously. With the addition of the compact 2DVD (which is capable of resolving spatial locations of drops to within less than 1 mm), this array then allows us to investigate rainfall spatial variability through five orders of magnitude, most of which have not been extensively explored in past studies.

Each LPM was calibrated in a separate indoor laboratory and moved to the field site. This study uses data taken by 19 operational LPMs (LPMs L and M had glitches in the wiring that were not rectified until early December).

The Thies LPM instruments were characterized in detail by de Moraes Frasson et al. (2011) and have been used in a number of other studies including Brawn and Upton (2008) and Fernández-Raga et al. (2009, 2010). Optical disdrometers are well recognized as useful tools for characterizing drop size distributions (e.g., Löffler-Mang and Joss 2000; Tokay et al. 2001). It is not likely that the results presented here depend upon the type of disdrometer (Islam et al. 2012b). The instruments are infrared occlusion instruments that can be run in several separate modes; for this study, the instruments were run in their default mode associated with 1-min integrations; in this mode, the device reports a spectrum each minute indicating how many droplets were detected in each of 22 disjoint drop size bins and 20 disjoint velocity bins (thus, each drop is characterized as belonging to one of 440 different categories). The known issues associated with particle sizing were mitigated to the greatest degree possible by verifying consistent performance in the laboratory before deployment and using identical instruments throughout the array. Moreover, measurements by all of the instruments were compared to minimize the inclusion of questionable behavior.

The devices are naturally synchronized; all devices were turned on simultaneously since they are powered with the same power supply. Although these devices are intended to be very low maintenance, the acquisition of data is reset every week to ensure minimal temporal drift; empirical estimation from this process suggests a relative shift of less than 1 s week^{-1} among all detectors. During the weekly maintenance activity, the devices are confirmed to be level, free of debris/insects, and recording properly.

The instruments are placed along three arms: two being orthogonal and the third bisecting the right angle. Eight instruments are spaced logarithmically out to 100 m along two of the arms, but the third arm, having seven instruments, only extends 52 m. This spacing provides increasing spatial resolution toward the network origin. One-minute drop counts over 22 size bins are recorded every minute for all the instruments so that we can estimate the PSDs for all the detectors every minute.

From this entire grid extending out to 100 m, grids of other sizes can be constructed as well. In this study we consider a 2-m grid (detectors A, B, H, Q), a 4-m grid (A, B, H, Q, C, J, R), and a 7-m grid (A, B, H, Q, C, J, R, D, K, S) as well as the full grid containing all of the instruments out to 100 m. Other grids can, of course, be constructed, but because we wished to look at the changes associated with the expansion of a network size rather than its relocation, we have the larger grids containing the smaller subgrids.

b. The effect of a network on the relative dispersion

As mentioned above, in this work the variability of a PSD is characterized by the relative dispersion of the distribution of $P(D)$ at each drop size. We denote this distribution of $P(D)$ at each size by $P(P_D \mid D)$ where the vertical bar denotes "at D." In Fig. 3 we illustrate one distribution $P(P_D \mid D)$ of values observed at the indicated drop size (black line). In this case, there is near full occupancy of the network since $P(P_D \mid D)$ at zero is very small. That is, during the 440 one-minute observations over all 19 detectors, the average $P(P_D \mid D)$ at this size was almost never close to zero. In part that is because these small sizes are ubiquitous, but for larger, scarcer drops, that is not necessarily true. To illustrate a more porous rain—that is, rain with voids at that size—we take this observed distribution and modify it to simulate only 60% occupancy or, to put it another way,

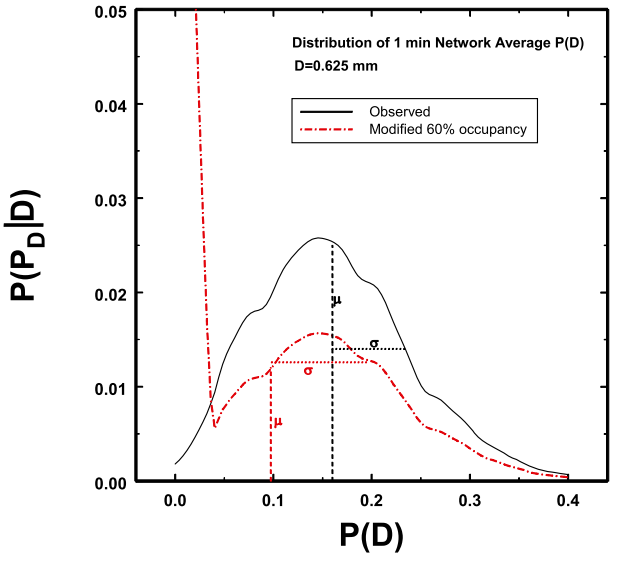

FIG. 3. The probability distribution by $P(P_D \mid D)$ of $P(D)$ showing the observations (black) and the results had 40% of the network been devoid of drops of this size (red). The mean μ and standard deviation σ illustrate that the relative dispersion would have increased $R_D = \sigma/\mu$ in this latter case.

40% of the time there were very few if any drops of this size in the entire network so that the network average was smaller than the smallest bin size of $P(D)$ used to compute $P(P_D \mid D)$. As Fig. 3 illustrates (red lines), both the mean μ and the standard deviation σ are altered with the latter increasing and the former decreasing. Consequently, the relative dispersion, $R_D = \sigma/\mu$, increases with decreasing occupancy. Thus, in general for each size, R_D over a network will be larger than R_{Di} [i.e., the value of the relative dispersion of $P(P_D \mid D)$ for the intrinsic PSD at size D].

The results depicted in Fig. 3, however, can be expressed explicitly. Consider a network having M detectors. Suppose that m of these have a very small $P(D) \le \varepsilon$, and suppose that the other $(M - m)$ values have an average $P(D) = \overline{x}$ and $P(D)^2 = \overline{x^2}$. Then it follows that

$$\mu = \frac{m\varepsilon + (M-m)\overline{x}}{M} \quad \text{and}$$

$$\overline{X^2} = \frac{m\varepsilon^2 + (M-m)\overline{x^2}}{M}, \tag{1}$$

where μ is the mean and $\overline{X^2}$ is the average squared value. It then follows that

$$R_D^2 = \frac{\overline{X^2}}{\mu^2} - 1 = \frac{Mm\varepsilon^2 + M(M-m)\overline{x^2}}{m^2\varepsilon^2 + 2m\varepsilon(M-m)\overline{x} + (M-m)^2\overline{x}^2} - 1. \tag{2}$$

As $\varepsilon \to 0$ and defining the fraction of detectors occupied as $f = (M - m)/M$,

$$R_D = \sqrt{\frac{1}{f}R_{Di}^2 + \frac{1-f}{f}}, \quad \text{where} \quad 1/M \le f \le 1. \tag{3}$$

Consequently, as $f \to 1$, $R_D \to R_{Di}$. On the other hand, as $f \to 1/M$, its smallest value, $R_D \to \sqrt{M-1}$ since for one grid value $R_{Di} \to 0$ so that R_D becomes only a function of the total number of detectors. This relation is plotted in Fig. 4 where it is clear that $R_D > R_{Di}$ for all $f < 1$.

Note that the M detectors can be distributed over an area of any size. The effect of different sizes of areas, then, is expressed through f, which depends on the sparseness of the rain. As we shall see, it also depends upon drop size so that, in reality, R_D never approaches R_{Di} simultaneously over all the drop sizes. Because the relative dispersion is a measure of the spread of probabilities around the average $P(D)$ at each size, this means that it is less likely that $P(D)$ will simultaneously be near their mean (intrinsic) values at all D. In that sense, the intrinsic PSD is less likely to be realized spatially over a network so that simply using a mean PSD and its associated R_{Di} is misleading particularly if measured by one instrument over time.

3. Data and analyses

a. An initial observation

With these tools, we begin the analyses of a rain event consisting of both a more intense component and a lighter component that began at 1645:00 UTC 23 Nov 2013 (Saturday) and lasted for 440 min with maximum rainfall rates approaching 250 mm h^{-1}. To get a basic feeling for this rain event, the rainfall rate averaged over the entire network is illustrated in Fig. 5. Only 19 of the 21 detectors were operational during this event (i.e., excluding detectors L and M as shown in Fig. 2) so that this average is only over those disdrometers. While for the most part we consider all 440 min, we also analyze two selected time periods as indicated with the red portion denoting the more intense rain and the green denoting the lighter rain. Each is 120 min long.

Given the above discussion, then it should come as no surprise that $P(D)$ could vary considerably from minute to minute over a network. Indeed, Fig. 6a illustrates the differences even between neighboring detectors A and B separated only by 1.93 m as previously shown in Fig. 1c. While the green areas denote $P(D)$ values that are nearly the same for the two detectors, detector A

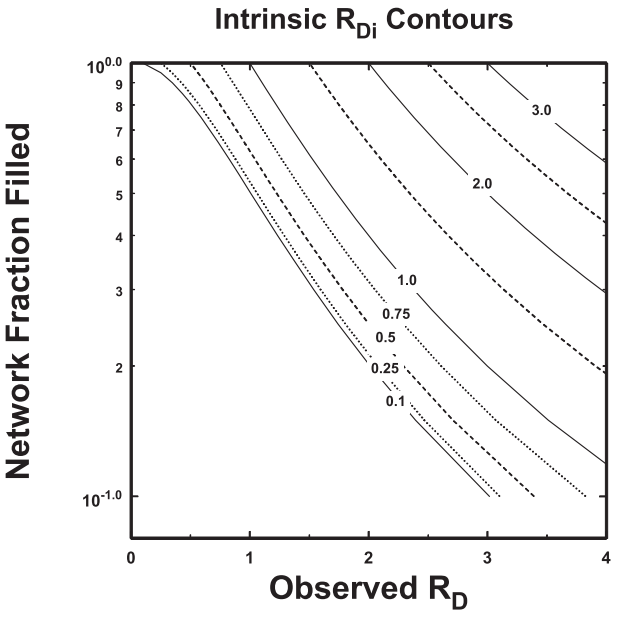

FIG. 4. Contours of R_{Di} as a function of R_D and the fraction of the network occupied by the drops. Note the increase in R_D for a fixed R_{Di} as the fraction filled decreases.

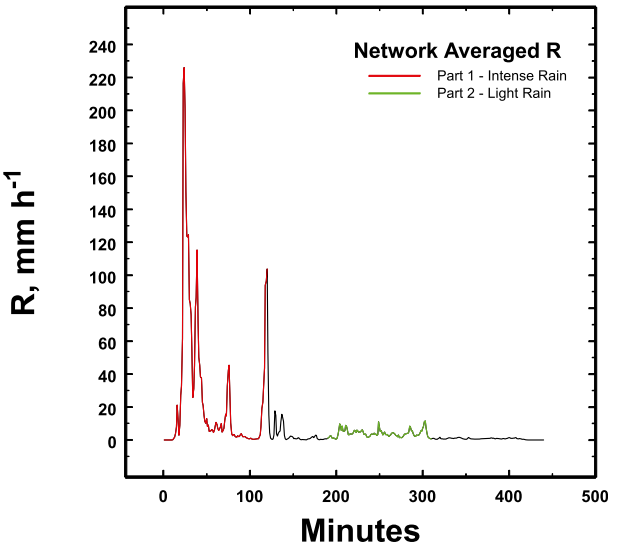

FIG. 5. The network-averaged rainfall rate for the (a) intense rain and (b) light rain as discussed in the text.

often showed greater $P(D)$ at the larger sizes, with the opposite being true at the smaller diameters. This, of course, could be due to subtle differences between the instruments, both of which were calibrated in the laboratory before deployment. However, even after computing the average $P(D)$ over the 2-m grid containing four detectors all lying within 1.93 m of detector A, there is still considerable variability in time at larger sizes as shown in Fig. 6b. One can also sense the increasing variability (relative dispersion) with increasing size by the spikiness. The same variability and trends with increasing diameters in the average $P(D)$ persists even when considering the entire 100-m network as illustrated in Fig. 6c. Yet all three examples show persistence in many of the overall structures in time regardless of the size of the network suggesting that the variability is real.

Indeed, these points are well illustrated in Fig. 7. With the exception of the very largest drop sizes, it appears that the mean values of $P(D)$ (solid lines) are strikingly similar regardless of the size of the network. What is clearly different are the relative dispersions (dotted–dashed lines) showing the variability of a 1-min PSD over different sizes of networks. As one would expect, while R_D for a single instrument can be quite substantial (magenta line), this potential variability is significantly reduced after averaging over several detectors in a network. For example, the peak R_D of 8.2 observed at the largest sizes by one detector is reduced by $1/\sqrt{19}$ to 1.92 as observed over all 19 instruments. This would seem to suggest that the variability is entirely due to sampling.

However, that turns out not to be correct because for over a 2-m network of $M = 4$ detectors, R_D actually decreases even more than for 19 detectors. Sampling would suggest R_D should have increased to 4.1, not decreased to 0.8. Something else is happening. Given the discussion concerning the fractional occupancy effect, this could be explained simply if the fractional occupancy f increased with decreasing network size as (3) requires. Then for the same R_{Di}, it would be possible for R_D to decrease even further even though there are fewer instruments. However, that is not what is happening to $f = (M - m)/M$, where m is the number of "no count" detectors out of M instruments in the network.

Instead, we see in Fig. 8 that the fractional occupancy is actually increasing with increasing network size. This would imply that R_D should decrease toward R_{Di} as the network size increases. Instead, Fig. 7 shows it increasing with increasing network size. Hence, we must conclude that R_D is actually increasing with increasing network size for a different reason. In other words, as a network extends over a larger area, the natural variability in $P(D)$ actually increases in spite of any $1/\sqrt{M}$ instrument effect.

b. A physical interpretation

This can be understood in terms of the spatial spectrum of drop concentrations or counts n as discussed and calculated in Jameson et al. (2015). Because $n = N_t \times P(D \mid D)$, the spectrum of n is identical to that for $P(D \mid D)$. That is, at each drop size there is

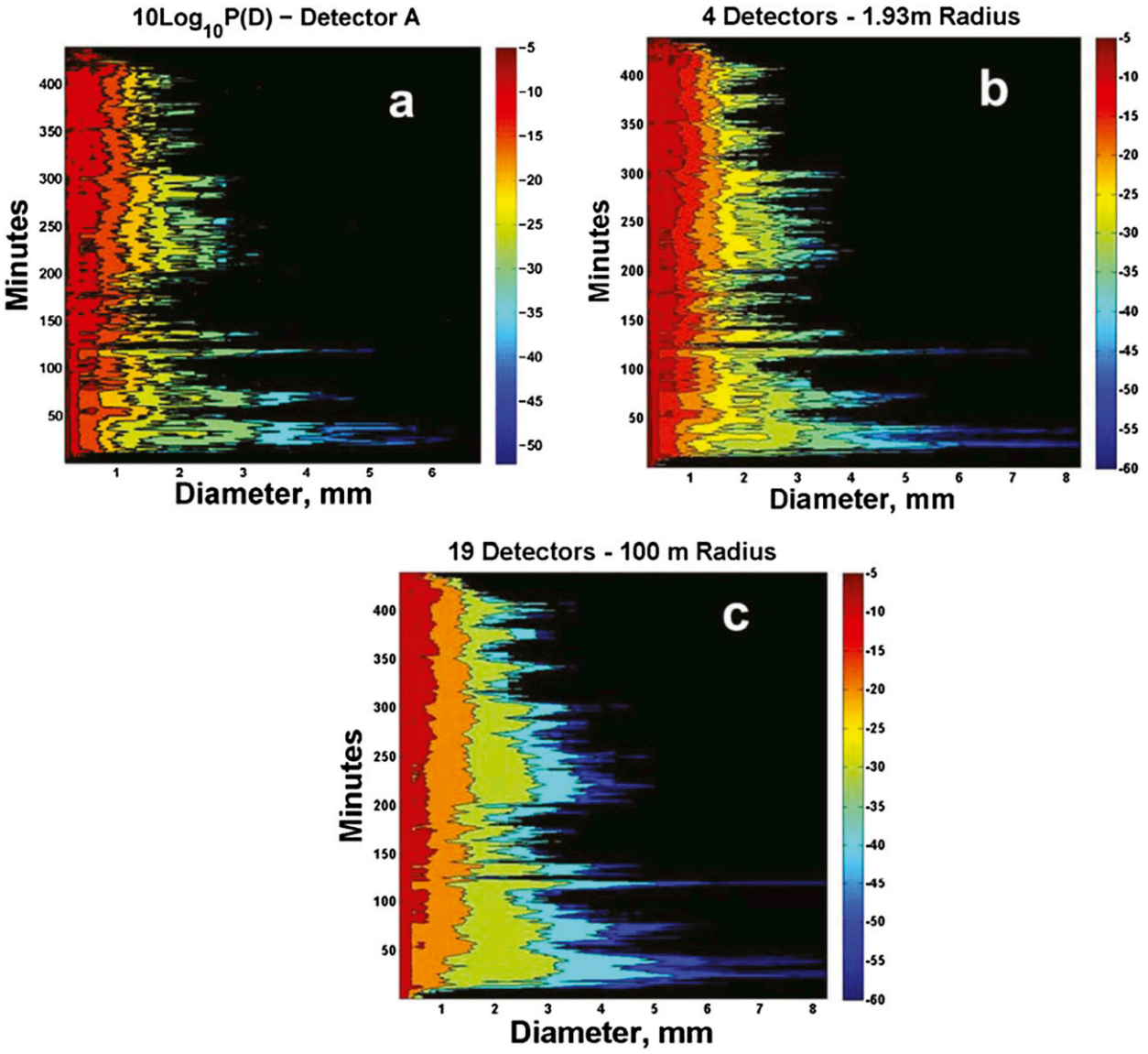

FIG. 6. Contour plots of $P(D)$ for (a) detector A as in Fig. 1a, (b) $10\log_{10}P(D)$ over four detectors within a radius of 1.93 m from detector A, and (c) $10\log_{10}$ of the network-average $P(D)$ over the entire network illustrating the effect of network (area) size.

a mean concentration, but the variance of the concentration produces the variance in $P(D)$ as well as in R_D. Given a reasonable number of detectors to adequately sample over the area, the physical reason for the increased variance is that as the area sampled by a network increases, the contributions to the variance by all spatial wavelengths in the part of the spectrum being sampled also increases. If we just consider a simple sinusoidal wave having amplitude a_i modulating around the mean concentration, the variance will be proportional to $|a_i|^2$. As the dimension of the area increases, the net variance will be proportional to the sum of all the amplitudes weighted by their spectral contributions. Hence, as the dimension of the area increases, the net variance will increase monotonically. Consequently, R_D will increase as the size of the area increases at least up until a wavelength of about ½ the characteristic dimension of the area if such wavelengths are present. While this cutoff is not rigid, longer wavelengths contribute mostly to the mean value, which is subtracted when computing the variance. Another way to think of it is that the network acts to integrate the Fourier transform of the spatial correlation function from the highest (smallest) toward lower (longest) frequencies (wavelengths) as the dimension of the network increases. Hence, this finding is quite general and not peculiar to this particular set of measurements.

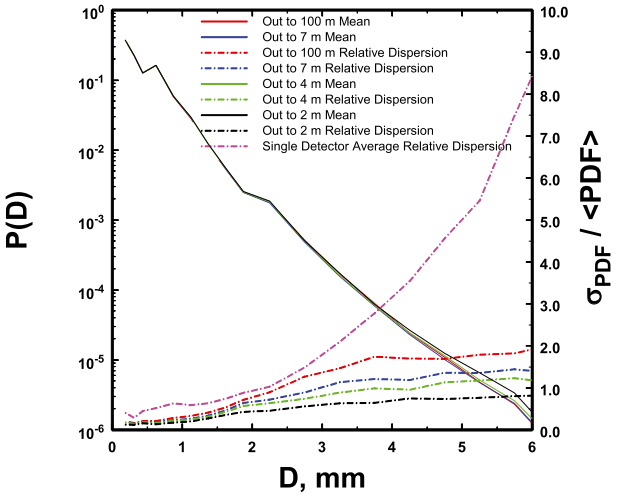

FIG. 7. The intrinsic $P(D)$ averaged over different sizes (areas) of networks (solid lines) and the observed total R_D for the different networks as functions of drop size over the 440 min of observations. Note the increase in R_D with increasing network size (area) and the similarities among the average PSDs.

Moreover, this understanding can also explain why R_D increases with increasing drop size for a fixed area covered by a network. The spatial distribution of drops is patchier (i.e., the drops occur more locally with more and larger gaps in between) as drop size increases (e.g., Jameson et al. 2015). Characterization of this patchier spatial distribution, then, requires greater spatial spectral widths as is well known from Fourier transform theory. Consequently, for the reasons given above, the variances must also increase as drop size increases. This effect is further amplified by the tendency toward lower mean $P(D)$ with increasing drop size so that the net effect is an increase in the relative dispersions as the drops become larger just as is observed.

In turn, this implies that the total variability of the distribution over a network should also increase. One measure of this total variability is the sum of the relative dispersions over all drop sizes as illustrated in Fig. 9. Obviously, the total variability increases monotonically with increasing dimension of the network. While this can be well fit parametrically by a power law, the ranges of the variables are too small to allow any physically reliable interpretation, and one should certainly not extrapolate to dimensions greater than those of the observations. This also suggests that if one had access to the full relevant spatial spectrum (i.e., Fourier transform of the spatial correlation function), in a particular situation, it might be possible to calculate how the total variability would scale with the size of an area. Unfortunately, such information is not readily available.

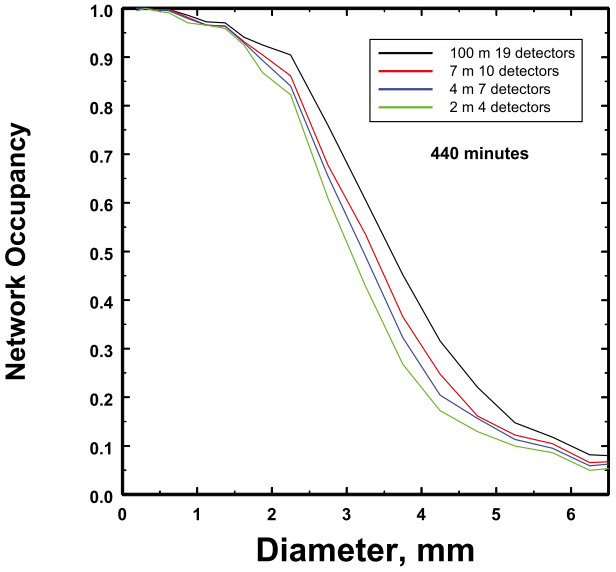

FIG. 8. Plots of the total fraction of the network filled during the entire period of observation as a function of drop diameter. Note that the fraction occupied actually increases as the network size (area) increases so that it cannot explain the observed increase in R_D with increasing network size (area).

c. Further analyses

Naturally, as one would expect, this same effect appears to be true regardless of the meteorology as illustrated in Fig. 10, where we subdivide the data into more intense or lighter rain. The same network size (area)

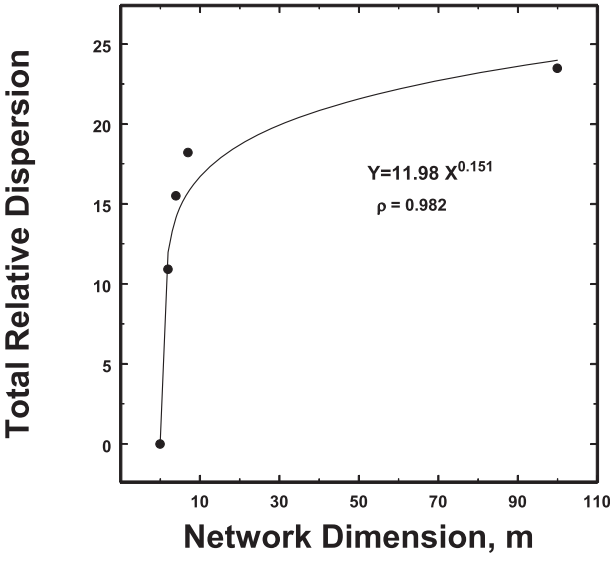

FIG. 9. The total relative dispersion (total variability) of the size probability distribution over the network plotted as a function of network dimension calculated by summing over all drop sizes. While this can be well fit parametrically by a power law, the ranges of the variables are too small to allow any physically reliable interpretation.

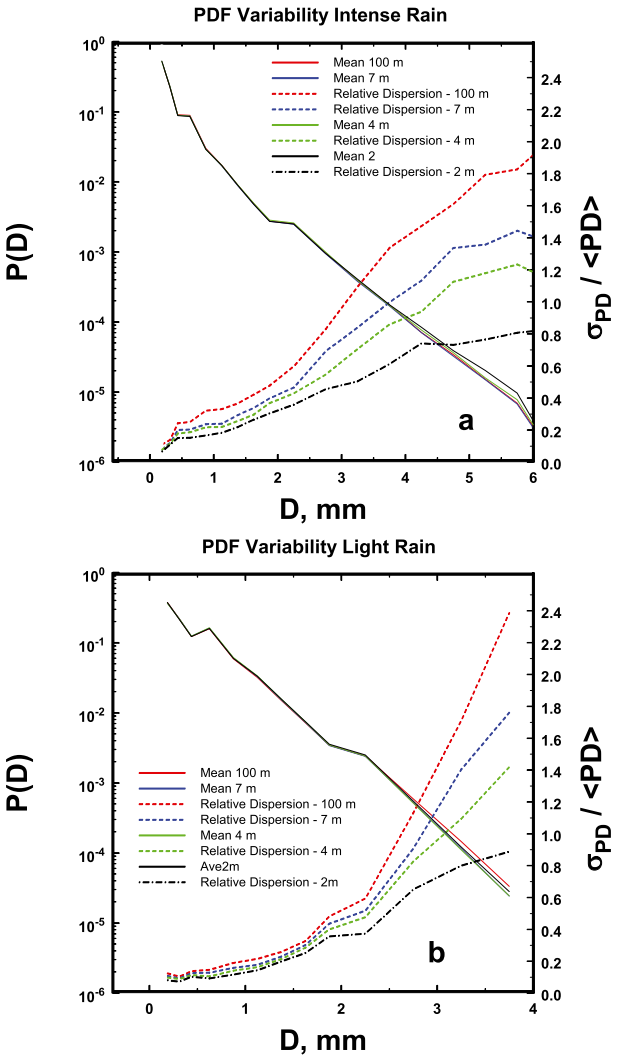

FIG. 10. As in Fig. 7, but for (a) the more intense rain and (b) the more stratiform rain noted in Fig. 5.

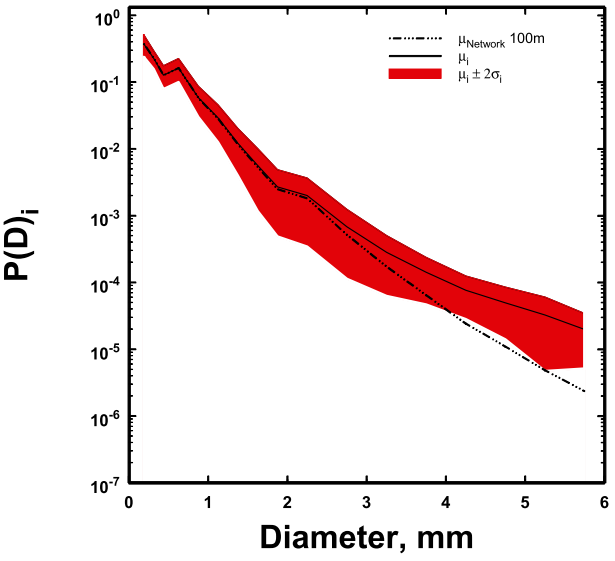

FIG. 11. Plots of the average intrinsic PSD and that observed over the entire network. The red-filled area illustrates the spread associated with the intrinsic PSD. Note that the mean curve for the entire network falls outside this region for drops larger than 4-mm diameter.

effect on the relative dispersion is apparent in both instances, as would be expected given the above discussion. There are some differences between the lighter and more intense rain, of course, as one would expect for different spatial spectra.

Clearly and, in retrospect, not surprisingly, these results imply that there can be a significant scatter of observed PSDs about any overall mean PSD. This is well illustrated in Fig. 11, where the 2σ bounds about the intrinsic average PSD are plotted. While this bounded area appears to be a reasonable size, the behavior of the network-average $P(D)$ (dotted–dashed line) at larger drop sizes suggests that such a conclusion fails to capture all of the variability over an area (network).

Indeed, just knowing a mean intrinsic PSD has its limitations with regard to the anticipated variability over an area. That is, one should expect that fluctuations in integrated variables such as R, Z, and the kinetic energy available for soil erosion should exceed what would be implied if one just considered fluctuations in the mean intrinsic PSD. That is, the natural variability of these variables is larger when the intrinsic PSD is spread out over areas because of the effects of spatial variability. Unfortunately, this is typically ignored in such calculations.

So what is more representative of the actual variability over a network (area) since Fig. 11 is incomplete? To reduce the effects of randomness in the sampling, one way to address this question is to consider time-average observed network PSD. Here we will consider 20-min network-average PSD. For the 440-min period of observations, this provides only 22 observed PSDs over the network, however. While useful, such a limited set is unlikely to capture the full potential real variability implied by the set of observations. To expand the size of a set of potential PSDs, we use the observed network time series of drop counts to define the distribution of mean drop counts using Bayesian analyses (Jameson 2007). In addition, the network-average temporal correlation functions at each size can be computed. These two components are then used to expand the size of the observed set of data in a manner consistent with the observed counts at all the drop sizes and with the observed correlation functions as explained in detail in Jameson (2015).

While the reader is referred to these latter references for a more complete discussion, we briefly describe the

procedure here. For each observed count of particles of a specified size, the application of the Bayesian approach under an assumption of counting statistics (Poisson or Gaussian, for example) produces a distribution of mean values of counts per unit observation interval. The most frequent mean values then emerge naturally as the most likely (ML) values surrounded by an estimate of the entire probability density function (pdf) of these mean values. Zeroes are included in this distribution to account for the frequency of data voids at each size during the observations.

The correlation among drops of the same size is described by the appropriate correlation function, usually an exponential having the correct $1/e$ correlation length, where e is the Euler number. In this work the cross correlation among drops of different sizes is not directly considered but instead arises naturally by applying the autocorrelation function for each different drop size to the same field of random numbers as described and demonstrated in Jameson (2015). This correlation of counts can be interpreted as a description of the meteorological ''structure,'' which, in turn, is a reflection of whatever physical processes produced it. A detailed knowledge of the meteorology is not required to use the correlation information. At each drop size, these correlation functions are then applied to an uncorrelated string of unit variance numbers uniformly distributed over [0, 1]. These correlated numbers are then used to generate a string of correlated drop counts at each size using the observed distributions of the mean counts and using the copula statistical technique. This technique is described in some detail with the appropriate references in Jameson (2015) and will not be repeated here. It should be noted that different random strings yield different sets of counts. This approach, then, makes it possible to form additional PSDs not actually observed but still consistent with the actual measurements. In effect, this approach provides a much fuller expression of all of the information contained within the observed correlations and drop counts than is given by just the realizations actually observed.

Using this approach for two different strings of random numbers, two sets each of 40 000 one-minute network counts at each drop size bin are generated. This now gives us 4000 additional 20-min PSDs that are consistent with the original set of data. In Fig. 12, these PSDs (gray) are plotted along with the observed (blue) 22 twenty-minute-average PSDs. Obviously, both the observed and simulated network 20-min-average PSDs show considerably greater variability than the R_{Di} associated with the intrinsic PSDs would imply. This is important because it means that collecting measurements over an area does not necessarily lead to less

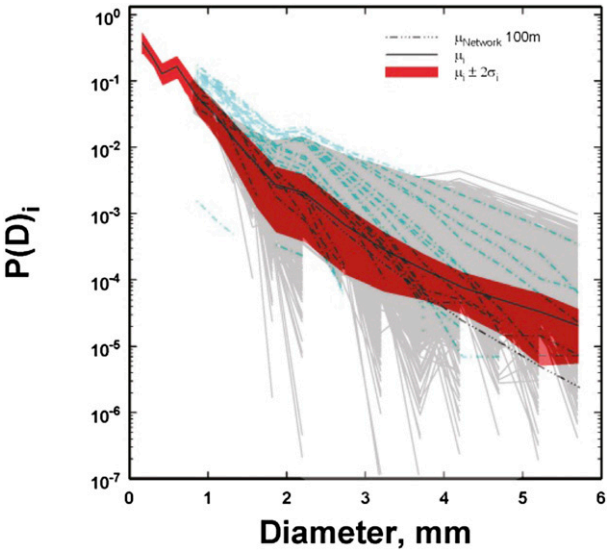

FIG. 12. As in Fig. 11, but with overlays of observed 20-min PSDs (blue lines which become black in the red areas) and simulated 20-min-average PSDs (gray) derived from the expanded dataset as discussed in the text. Note the much greater network variability compared with that for the intrinsic PSD.

spread in the estimated PSDs even though many more instruments are included.

Moreover, this variability seems to increase significantly beyond about 1.5-mm diameter. To show this more clearly, the time-averaged network-relative dispersions as a function of drop size are plotted in Fig. 13. The observed values increase with increasing network size (area) and with increasing drop size at least up to 2–3-mm diameters. Beyond that, the average relative dispersion appears to decline. This is somewhat surprising given the earlier discussion above (i.e., increased patchiness and lower mean probabilities at larger sizes). To explore why this might be happening, we take the simulation results and compute the network-averaged R_D over time. This yields about 2000 samples as compared to the observed 50–100 samples at the larger drop sizes. If controlled simply by sample statistics, this would suggest a decrease in R_D by over a factor of 4. However, the opposite occurs as illustrated by the dotted–dashed curve in Fig. 13.

Despite the much larger samples corresponding to the simulation, the relative dispersion actually increases monotonically for drop sizes greater than 1-mm diameter as we would expect and in contrast to the direct but apparently misleading observations. We believe, then, that this difference reflects an inadequate sampling of the physics by the set of observations. This phenomenon has been observed before, such as when investigators attempt to use a limited set of disdrometer observations to compute the so-called Z–R relations

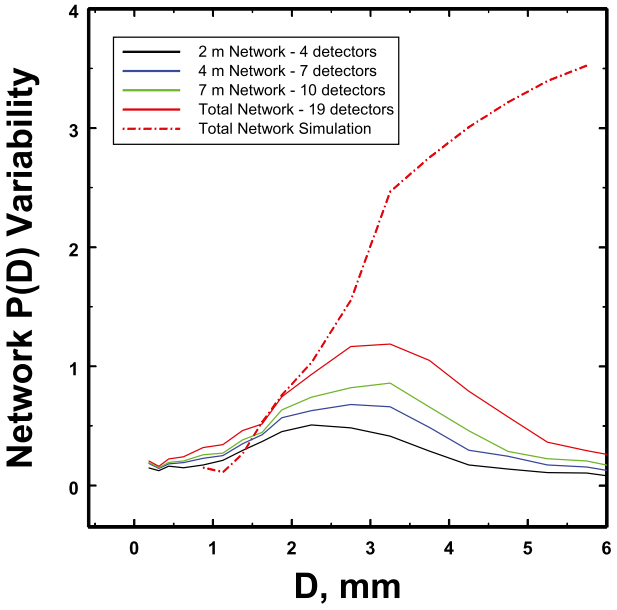

FIG. 13. The 1-min-average R_D over the entire observation period as functions of the drop size and network size compared to that for the expanded dataset. The rolloff at larger drop sizes is attributed to incomplete sampling by the observations as discussed in the text.

prevalent throughout radar meteorology (Jameson and Kostinski 2002) and to deduce correlations among parameters (e.g., Jameson 2015, Fig. 12 therein). There, it was found that false correlations and data misfits occurred because of an extreme undersampling of the number of drops. The effects of this undersampling of the physics could, in part, be alleviated using a dataset expanded along the approach outlined above (e.g., Jameson 2015). The observations, after all, are just a limited set of realizations from the rich statistical processes described more completely by the correlation functions and distributions of mean counts for the different drop sizes. The simulation, then, provides access to many more of the possibilities than just those sampled in the observations. Apparently, this can be important at times.

4. Summary

As discussed above, a drop size distribution can be expressed as DSD $= N_t \times P(D) = N_t \times$ PSD. The variability of PSD is then defined by the distribution of probabilities $P(P_D \mid D)$ at each drop size and is investigated over a network of optical disdrometers. It was found that the variability as measured by the relative dispersions R_D of $P(P_D \mid D)$ as functions of drop size increases with increasing size of the network and with increasing size of the drops. Furthermore, the variability over a network is often significantly greater than that implied by the intrinsic PSD—that is, the PSD deduced from one or more instruments after excluding all zero drop counts.

Both of these observations can be explained in terms of the spatial spectrum of $P(D)$. That is, each component of such a spectrum contributes to the variance and to the R_D. As a network size (area) increases, more spectral components contribute, thus increasing R_D since the average $P(D)$ remains fixed. Another way to think of it is that the network acts to integrate the Fourier transform of the spatial correlation function from the smallest toward larger wavelengths as the dimension of the network increases. Likewise, the spatial distribution of raindrops becomes spikier or patchier as the drop size increases. From classic Fourier transform theory, this, in turn, implies a greater number of spatial spectral components in order to characterize this spatial distribution so R_D increases with increasing drop size. These observations, then, suggest that if one has access to a characterization of the spatial spectrum of the rain (i.e., the Fourier transform of the spatial correlation function), it should be possible to apply an intrinsic drop size distribution properly over an area. In the absence of that information, however, the intrinsic PSD and R_{Di} will underestimate the true areal variability. Of course, it must also be remembered that time averaging tends to reduce the variability due to sampling fluctuations, but it does not necessarily eliminate or smooth out the true physical variability (e.g., Jameson et al. 2015).

Finally, as observed in previous studies, care must be taken that the physics is being properly sampled. Even though 1-min measurements over 19 detectors for 440 min sounds like a lot of data, it was found that even that amount of information did not provide a full characterization of the likely true variability of the PSD without additional expansion of the set of observations because the observations themselves represent only one realization of multiple stochastic processes. It must also be remembered that in this work we have ignored the variability of the total number of drops, which also contributes significantly and probably dominantly to the variability of the rainfall rate and other integrated parameters as previously recognized by Jameson and Kostinski (2001).

Acknowledgments. This work was supported by the National Science Foundation (NSF) under Grant AGS130087 as well as by the United States Social Security Administration. Support for ML came from the National Science Foundation under Grant AGS-1230240. Support for AK came from NSF Grant AGS-111916. The authors are also especially grateful to the

students of Prof. Larsen, namely Joerael Harris, Robert Lemasters, Katelyn O'Dell, Joshua Teves, and Michael Chute who diligently worked to make this network a functioning reality.

REFERENCES

Best, A. C., 1950: The size distribution of raindrops. *Quart. J. Roy. Meteor. Soc.*, **76,** 16–36, doi:10.1002/qj.49707632704.

Brawn, D., and G. Upton, 2008: On the measurement of atmospheric gamma drop-size distributions. *Atmos. Sci. Lett.*, **9,** 245–247, doi:10.1002/asl.198.

de Moraes Frasson, R. P., L. K. da Cunha, and W. F. Krajewski, 2011: Assessment of the Thies optical disdrometer performance. *Atmos. Res.*, **101,** 237–255, doi:10.1016/j.atmosres.2011.02.014.

Fernández-Raga, M., A. Castro, C. Palencia, A. Calvo, and R. Fraile, 2009: Rain events on 22 October 2006 in León (Spain): Drop size spectra. *Atmos. Res.*, **93,** 619–635, doi:10.1016/j.atmosres.2008.09.035.

——, and Coauthors, 2010: The kinetic energy of rain measured with an optical disdrometer: An application to splash erosion. *Atmos. Res.*, **96,** 225–240, doi:10.1016/j.atmosres.2009.07.013.

Islam, T., M. A. Rico-Ramirez, D. Han, and P. K. Srivastava, 2012a: Using S-band dual polarized radar for convective/stratiform rain indexing and the correspondence with AMSR-E GSFC profiling algorithm. *Adv. Space Res.*, **50,** 1383–1390, doi:10.1016/j.asr.2012.07.011.

——, ——, ——, and ——, 2012b: A Joss–Waldvogel disdrometer derived rainfall estimation study by collocated tipping bucket and rapid response rain gauges. *Atmos. Sci. Lett.*, **13,** 139–150, doi:10.1002/asl.376.

——, ——, M. Thurai, and D. Han, 2012c: Characteristics of raindrop spectra as normalized gamma distribution from a Joss–Waldvogel disdrometer. *Atmos. Res.*, **108,** 57–73, doi:10.1016/j.atmosres.2012.01.013.

Jaffrain, J., and A. Berne, 2012a: Influence of the subgrid variability on the raindrop size distribution and radar rainfall estimators. *J. Appl. Meteor. Climatol.*, **51,** 780–785, doi:10.1175/JAMC-D-11-0185.1.

——, and ——, 2012b: Quantification of the small-scale spatial structure of the raindrop size distribution from a network of disdrometers. *J. Appl. Meteor. Climatol.*, **51,** 941–953, doi:10.1175/JAMC-D-11-0136.1.

Jameson, A. R., 2007: A new characterizations of rain and clouds: Results from a statistical inversion of count data. *J. Atmos. Sci.*, **64,** 2012–2028, doi:10.1175/JAS3950.1.

——, 2015: A Bayesian method for upsizing disdrometer drop size and counts for rain physics studies and large scale applications. *IEEE Trans. Geosci. Remote Sens.*, **53,** 335–353, doi:10.1109/TGRS.2014.2322092.

——, and A. B. Kostinski, 2001: Reconsideration of the physical and empirical origins of *Z–R* relations in radar meteorology. *Quart. J. Roy. Meteor. Soc.*, **127,** 517–538, doi:10.1002/qj.49712757214.

——, and ——, 2002: Spurious power-law relations among radar and rainfall parameters. *Quart. J. Roy. Meteor. Soc.*, **128,** 2045–2058, doi:10.1256/003590002320603520.

——, M. L. Larsen, and A. B. Kostinski, 2015: Disdrometer network observations of fine scale spatial/temporal structures in rain. *J. Atmos. Sci.,* doi:10.1175/JAS-D-14-0136.1, in press.

Jones, D. M. A., 1956: Rainfall drop size distributions and radar reflectivity. ISWS Research Rep. 6, Illinois State Water Survey, 20 pp.

Kostinski, A. B., and A. R. Jameson, 1999: Fluctuation properties of precipitation. Part III: On the ubiquity and emergence of exponential size spectra. *J. Atmos. Sci.*, **56,** 111–121, doi:10.1175/1520-0469(1999)056<0111:FPOPPI>2.0.CO;2.

Laws, J. O., and D. A. Parsons, 1943: The relation of raindrop size to intensity. *Trans. Amer. Geophys. Union,* **24,** 452–460, doi:10.1029/TR024i002p00452.

Lee, C. K., G. W. Lee, I. Zawadzki, and K.-E. Kim, 2009: A preliminary analysis of spatial variability of raindrop size distributions during stratiform rain events. *J. Appl. Meteor. Climatol.*, **48,** 270–283, doi:10.1175/2008JAMC1877.1.

Lee, G. W., and I. Zawadzki, 2005: Variability of drop size distributions: Noise and noise filtering in disdrometric data. *J. Appl. Meteor.*, **44,** 634–652, doi:10.1175/JAM2222.1.

Löffler-Mang, M., and J. Joss, 2000: An optical disdrometer for measuring size and velocity of hydrometeors. *J. Atmos. Oceanic Technol.,* **17,** 130–139, doi:10.1175/1520-0426(2000)017<0130:AODFMS>2.0.CO;2.

Marshall, J. S., and W. M. Palmer, 1948: The distribution of raindrops with size. *J. Meteor.*, **5,** 165–166, doi:10.1175/1520-0469(1948)005<0165:TDORWS>2.0.CO;2.

Tokay, A., and P. G. Bashor, 2010: An experimental study of small scale variability of raindrop size distribution. *J. Appl. Meteor. Climatol.*, **49,** 2348–2365, doi:10.1175/2010JAMC2269.1.

——, A. Kruger, and W. F. Krajewski, 2001: Comparison of drop size distribution measurements by impact and optical disdrometers. *J. Appl. Meteor.*, **40,** 2083–2097, doi:10.1175/1520-0450(2001)040<2083:CODSDM>2.0.CO;2.

Wexler, R., 1948: Rain intensities by radar. *J. Meteor.*, **5,** 171–175, doi:10.1175/1520-0469(1948)005<0171:RIBR>2.0.CO;2.